Probability mapping images in dynamic speckle classification

Isabel Passoni,[1,3] Héctor Rabal,[2,4] Gustavo Meschino,[1,5] and Marcelo Trivi[2,6]

[1]Laboratorio de Bioingeniería, Facultad de Ingeniería, Universidad Nacional de Mar del Plata, Juan B. Justo 4302, Mar del Plata 7600, Argentina

[2]Centro de Investigaciones Ópticas (CONICET La Plata-CIC), UID Optimo, Departamento de Ciencias Básicas, Facultad de Ingeniería, Universidad Nacional de la Plata, Argentina, P.O. Box 3, Gonnet, La Plata 1897, Argentina

[3]e-mail: lpassoni@fi.mdp.edu.ar

[4]e-mail: hrabal@ing.unlp.edu.ar

[5]e-mail: gmeschin@fi.mdp.edu.ar

[6]e-mail: marcelot@ciop.unlp.edu.ar

Received 5 July 2012; revised 22 November 2012; accepted 12 December 2012; posted 12 December 2012 (Doc. ID 171231); published 30 January 2013

We propose the use of a learning procedure to identify regions of similar dynamics in speckle image sequences that includes more than one descriptor. This procedure is based on the application of a naïve Bayes statistical classifier comprising the use of several descriptors. The class frontiers can be depicted so that the proportion of identified regions may be measured. To demonstrate the results, assembly of an RGB image, where each plane (R, G, and B) is associated with a particular region (class), was labeled according to its biospeckle dynamics. A high brightness in one color means a high probability of the pixel belonging to the corresponding class, and vice versa. © 2013 Optical Society of America

OCIS codes: 030.6600, 110.6150, 100.4993.

1. Introduction

Dynamic speckle phenomena due to either biological or industrial samples usually show different behaviors when the surface is not homogeneous. Measurements of local activity can be used to recognize and show regions of similar activity [1] in heterogeneous samples. Interpretation of the results in terms of the physical origins that produce the dynamics has only been solved for a few cases. Doppler shifts and other time-varying phenomena compete to give rise to a complex time behavior that is hard to assign to simple reasons. Classification, identification, and measurement of regions with similar activities are important both for research and for industrial applications.

In the context of the classification of pixels based on their features, a class is a set of pixels that is similar (according to a specific criteria) in the feature space. Each class represents a different area in the image.

However, this task is not always easy, and some difficulties appear in classification or grouping in classes when using only one descriptor.

The time evolution of intensities of each pixel of a biospeckle $I(x, y, t)$ is a time series presenting a noisy appearance (see Fig. 1). Several features have been extracted from these time patterns, taking into account properties, such as the dynamic range, time-frequency features, long-term correlation tendencies, and fractal dimension, among others.

The space behavior of the dynamic speckle pattern is, in a certain sense, a texture, and so a huge set of descriptors might be used for its characterization. Haralick *et al.* suggest several different texture

1559-128X/13/040726-08$15.00/0

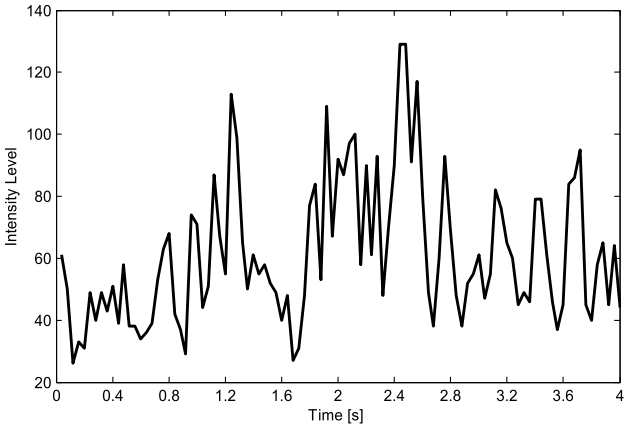

Fig. 1. Pixel intensity over time.

descriptors that have been used to describe speckle activity, and several others can be added [2].

Generally a single descriptor is not enough to characterize differences among speckle patterns. In particular, dealing with biological samples (fungi, bacteria, apples, corn, grains, fruits, and tissues) is more difficult than a surface phenomenon like a paint drying process when it comes to phenomena characterization.

Different phenomena show different behaviors, and it is not easy to classify their profiles as belonging to a single class. Several descriptors have been defined in the literature, for example, spectral bands [3], Fujii measure [4], wavelet entropies [5], fuzzy granularity [6], morphological descriptors [7], Hurst coefficient [8], vortices [9], full width at half-maximum (FWHM) [10], cumulants [11] and other descriptors of the autocorrelation function [12], empirical mode decomposition [13], laser speckle contrast analysis (LASCA) [14], and dynamic range [15].

Each one has advantages and shortcomings for the characterization of different phenomena, some of which are commented upon next.

Dynamic range is very fast to compute and is insensitive to nonuniform illumination given the condition that the amplitude of the variation in the pattern is a linear function of the activity.

The Fujii method works in the temporal domain. It provides a good discrimination among regions if the image is uniformly illuminated, but the information that it provides may be misunderstood in regions with low illumination.

In the LASCA method a local contrast is estimated that does not require more than single frame with a carefully chosen integration time. As it requires operation on spatial windows, the spatial resolution is lower than in other methods. If the spatial windows do not overlap, a tiled image is generated.

Spectral bands work in the frequency domain, and their ranges permit discrimination of the activity of the sample in different frequency ranges. In this sense this approach is a multiple-descriptor one. It requires a high number of frames and thus cannot be applied to characterize nonstationary phenomena.

Vortices require very few frames (could be as few as two), and they are useful to characterize low activity, but it is difficult or impossible to implement it for higher activity levels.

The Hurst coefficient describes persistent or long-term correlations and is related to the fractal dimension. It requires many frames and high computational cost and cannot be used for nonstationary phenomena.

Cumulants, obtained from the autocorrelation of the pixel time history, have a well-defined physical meaning in terms of Voigt profile, Doppler broadening, and eventually the Wolff effect. It requires many frames and is not meaningful for nonstationary processes [16].

The FWHM of the autocorrelation function has also been employed [10] and shows similar features to cumulants.

Empirical mode decomposition demands high computational cost given the iterative process features, requires many frames, and in some cases assigns the same values to different types of activity.

In this paper we propose the use of more than one descriptor considering *a priori* knowledge and supervised learning. It uses known samples (as classified by an expert) to find the typical behavior of pixels of each class in order to characterize regions of a sample with different properties. We use a multivariate supervised classifier for obtaining an automatic process that optimizes decision making. In this case it is based on the recognition of a color plane, it could be implemented with a machine vision system, and the supervised classifier would be tuned for the detection of events of interest.

As an example we show (a) learning of the behavior of healthy regions, bruised regions, and inert regions in a bruised fruit and (b) application in the classification of different fruits of the same kind that were not included as data during the learning procedure.

The aim is then to improve classification, avoiding confusions between classes, and to identify regions with similar dynamics.

The classification problem involves the selection of features, in this case dynamic speckle descriptors, as well as an adequate classifier. The performance and some features of the different descriptors are described in [17] for morphologic ones and in [15] for some others.

Given that the phenomenon to be classified, i.e., to identify regions of similar activity, is highly dependent of the observed specimen, we propose the use of a supervised classifier. That is a classifier trained by using known behaviors. Specifically, we propose the use of the naïve Bayes classifier. In spite of its strict statistical requirements, it has shown great efficacy in a broad range of applications [18].

In order to select the set of descriptors with the lowest computational cost and in turn to achieve the best performance for the identification of the

phenomenon, we used the method of wrapping feature selection. In the example that we chose to illustrate the method, the set of descriptors is formed by dynamic range, Fujii descriptor, and wavelet entropy. This descriptor set blends a time-frequency descriptor (wavelet entropy) and two descriptors that work in the time domain (dynamic range and Fujii), given the best confusion matrix, as a quality assessment method.

Two different methods are proposed to display the classification results: one is the assembly of an RGB image, where each color plane (R, G, and B) is associated with the probability of belonging to a particular class (three classes, one per color plane). Each pixel of the RGB image has three components, each computed as an estimation of the probability of belonging to a particular class. The RGB color plane of each pixel is enhanced according to the probability of belonging to the corresponding class and vice versa. In this way the overlap of the memberships of different classes is shown as a combination of basic colors.

The other way of showing the results is by considering the naïve Bayes classifier outcome, which we present as a single-plane color image. Each pixel is colored with the hue associated with one particular class. This class is computed according to the combination of the Bayesian model with a decision rule that selects the most probable hypothesis of belonging to a class. Hence, in the results, every pixel shows a well-defined color that permits its analysis by visual inspection.

2. Description of the Method

A. Naïve Bayes Classifier

We propose a supervised approach to classify regions of images of speckle patterns according to the dynamic features of the observed phenomenon. In particular we address the naïve Bayes classifier, which as is widely known assigns the most likely class to a given sample described by its feature vector [18].

Let us define:

- $\mathbf{D}$ is a random variable vector whose values are vectors of feature values $\mathbf{D} = [d_j]_{j=1,\ldots,m}$.
- C is a random variable whose values are the classes c_k and $k = 1, \ldots, n$.
- $P(C = c_k/\mathbf{D} = \mathbf{d}) = P(c_k/\mathbf{d})$ is the conditional probability that a sample belongs to a class c_k, given that it has a feature vector $\mathbf{d}$.
- $P(\mathbf{D} = \mathbf{d}/C = c_k) = P(\mathbf{d}/c_k)$ is the conditional probability of obtaining a particular descriptor vector belonging to class c_k.
- $P(C = c_k)$ is the unconditional probability of obtaining a sample of c_k class.
- $P(c_k)$ is the *a priori* probability that a sample belongs to class c_k and $k = 1, \ldots, n$.

Using the Bayes' theorem, the probability of a sample belonging to a region on its descriptor basis is stated as

$$P(c_k/\mathbf{d}) = P(c_k) \times \frac{P(\mathbf{d}/c_k)}{P(\mathbf{d})}, \tag{1}$$

where

$$P(\mathbf{d}) = \sum_{i=1}^{n} P(c_i) P(\mathbf{d}/c_i). \tag{2}$$

Since $P(c_k/\mathbf{d})$ is unknown, the Bayes' rule combines the estimation of $P(\mathbf{d}/c_k)$, $P(c_k)$, and $P(\mathbf{d})$ to get an estimate of $P(c_k/\mathbf{d})$.

We assume that all possible events fall into exactly one of n classes. Also, the *a priori* probabilities $P(c_k)$ are unknown and variable according to the experiments. Therefore, to make them independent of the manual assignment of the training sample, we assume that prior probabilities $P(c_k)$ are equal. Therefore, we can write Eq. (1) including Eq. (2):

$$P(c_k/\mathbf{d}) = P(c) \times \frac{P(\mathbf{d}/c_k)}{\sum_{i=1}^{n} P(c) P(\mathbf{d}/c_i)} \Rightarrow P(c_k/\mathbf{d}) = \frac{P(\mathbf{d}/c_k)}{\sum_{i=1}^{n} P(\mathbf{d}/c_i)}. \tag{3}$$

The naïve Bayes model assumes that the occurrence of a particular value of any descriptor is statistically independent of the occurrence of any other one; hence, the distribution of $\mathbf{d}$ conditional on c_k can be decomposed as follows:

$$P(\mathbf{d}/c_k) = \prod_{j=1}^{m} P(d_j/c_k). \tag{4}$$

Then Eq. (3) becomes

$$P(c_k/\mathbf{d}) = \frac{\prod_{j=1}^{m} P(d_j/c_k)}{\sum_{i=1}^{n} \prod_{j=1}^{m} P(d_j/c_i)}. \tag{5}$$

An estimation of $P(d_j/c_k)$ can be approximated with relative frequencies by considering the *training data set*. To estimate the parameters of the feature's distribution, we propose generating nonparametric models, where their structure is determined from the data. The kernel density estimation is a data-smoothing technique where inferences about the population are made based on a finite data sample [19]. Having collected training samples of feature vectors corresponding to known classes, the *a priori* probabilities $P(d_j/c_k)$ are estimated.

If the problem addressed is the classification of image pixels that are limited to three classes, the result of each $P(c_k/\boldsymbol{d})|_{k=1,\ldots,3}$ is fed into a color channel of an RGB image. The RGB color model is an additive color model in which red, green, and blue light are added together to reproduce a broad array of colors. Thus, its ability to display midtones is exploited as a way to show the probability of belonging to the three classes. Thus, for example, a region that is seen in yellow is due to it simultaneously having a similar

membership level to the classes of the red and green channels.

When $P(c_k/\boldsymbol{d})$ is computed, classification can be optimally obtained. Hence, the expected number of misclassifications can be minimized by assigning a class with a feature vector $\mathbf{d}$ to the region c_k for which $P(c_k/\boldsymbol{d})$ is highest.

To obtain a single plane image, the combination of the Bayesian model with a decision rule is used. One common rule consists in selecting the hypothesis that is most probable; this is known as the maximum *a posteriori* (MAP) decision rule. The corresponding classifier is the function classify, defined as follows:

$$\text{classify}(d_1, ..., d_3) = \arg \max_c \frac{\prod_{j=1}^{n} P(d_j/c_k)}{\sum_{i=1}^{3} \prod_{j=1}^{n} P(d_j/c_i)}, \tag{6}$$

where "arg max" stands for argument of the maximum; that is to say, pixelwise, the maximum over the set of the three class probabilities.

B. Descriptor Selection

For each dynamic laser experiment several descriptors are computed from the image sequences on a pixelwise basis. Then a set of intensity images assembled with the descriptor values is built.

In order to test the performance of this method, we evaluate the segmentation of bruising regions of apples, which are not yet visible. It has been stated that this region exhibits different bioactivity with respect to the nonbruised ones [10].

For each class (pixels presenting similar activity levels), upon a set of regions of different samples selected by an operator over an image (regions corresponding to the classes to detect), a probability density function is estimated using a kernel density estimation approach. Hence, based on a finite data sample, inferences about the population are made with this estimation. In our example, we propose identifying three classes: bruised apple region, healthy apple region, and inert (control) zone.

The amount of possible descriptors is too large to run an exhaustive search process for obtaining a feature subset that satisfactorily performs the classification task. In order to choose the best descriptor subset to achieve the region identification, a wrapper feature selection algorithm based on a stochastic search process was run. A wrapper method considers the classifier inside the search process; i.e., the chosen features are appropriate to be used with the considered classifier, but it does not mean that they are optimal for other classification schemes [20].

We used a genetic algorithm as the search process, configured to maximize the classification rate (number of pixels successfully classified against the total number of pixels). In addition, we built a fitness function that favorably weighed the time-dependent descriptors in relation to those involving transformations in the frequency domain. This was done in order to reduce the computational cost, so, based on our previous heuristics, we tried to obtain only one frequency-based descriptor (for example, a wavelet-based one), and we gave more weight to time features than the other frequency features. These conditions were considered in the search process as constraints.

A subset of three descriptors was obtained using the above-mentioned wrapper method. These features capture the speckle dynamic over the range of intensities, displaying encouraging results to differentiate biospeckle activities regions in bruised fruits [12]. These are the difference between images and a spatial–temporal approach like the dynamic range, generalized differences or Fujii, and wavelet-based entropy.

Therefore, for the particular case of the classification of image sequences of apples, we segmented their areas into three classes: bruised, healthy and inert (control area, where any biospeckle activity is assured) regions.

1. *Dynamic Range [15]*

$$R_{x,y} = \max(I_{x,y,t}) - \min(I_{x,y,t}), \tag{7}$$

where max( ) and min( ) are the maximum and minimum values reached by the intensity of the pixel over time, respectively. This measure is similar to the maximum height of the profile used in surface roughness characterization.

Given that the dynamic range descriptor is sensitive to intensity amplitude and that the aim is to discover variations between regions, a scaling of the intensity image stack to the [0, 255] range must be previously performed. In this way it compensates for differences in the illumination conditions among experiments.

2. *Fujii [4]*

$$F_{x,y} = \sum_{n=1}^{N} \frac{|I_{x,y}(n) - I_{x,y}(n-1)|}{|I_{x,y}(n) + I_{x,y}(n-1)|}, \tag{8}$$

where $I_{x,y}(n)$ is the intensity level at (x,y) in frame n and $n = 1 \ldots N$ indicates the frame number in the image sequence. This measure has proven to be a very good estimation of activity when there are no local variations in the illumination of the sample.

3. *Discrete Wavelet Transform Shannon Entropy Descriptor [5]*

After the development of the time profile in each pixel in discrete wavelet transform coefficients C_j, the following wavelet-based entropy can be defined (which has been successfully applied in biospeckle characterization):

$$E_j^{(i)} = \frac{1}{N_j}\sum_k |C_j(k)|^2, \tag{9}$$

where $E_j^{(i)}$ is the mean energy at j scale in a temporal window i of the intensity over time, in the N_j discrete wavelet transform (DWT) coefficients in the resolution level j.

Then the total energy at window i is

$$E_{\text{total}}^{(i)} = \sum_j E_j^{(i)}, \tag{10}$$

and the relative energy at window i is

$$p_j^{(i)} = \frac{E_j^{(i)}}{E_{\text{total}}^{(i)}}. \tag{11}$$

Therefore, the Shannon entropy in the window is

$$S_{W_{x,y}}^{(i)} = -\sum_{j<0} p_j^{(i)} \cdot \ln[p_j^{(i)}]. \tag{12}$$

This measure describes how evenly energy is distributed among the different frequencies.

With these three descriptors as an example we plotted the continuous value of the pixel probability of each class. Then we arranged the three images (one per class) to build an *RGB color model image* (using the three planes).

Finally, by combining the probabilistic model with the MAP rule, we defined a classifier that detects the estimation of each pixel belonging to the class where the probability is at its maximum. This result is presented as an intensity image (gray scale).

3. Experimental Results

We conducted a series of experiments to assess the performance of the method. They were aimed to segment, by using an RGB color model, regions of the samples with different activities.

The experimental setup used to detect bruising in apples [5,8,12] is shown in Fig. 2.

An expanded low-power He–Ne laser (5 mW) illuminated the apple, and successive subjective speckle images were registered by a CCD camera ($f = 50$ mm, $f/n = 16$). A set of 100 images (300×300 squared pixels) was digitized to 8 bits and stored in a computer. For the training stage we used the same experimental data as in [5,8,12]. A constant 25 Hz sampling frequency was used, and the camera integration (exposure) time was set to 40 ms.

Bruising that could not be detected by visual inspection was produced on an otherwise healthy apple by letting a sphere fall on it (diameter, 21.9 mm; weight, 133.6 g; height, 20 cm), and an inert object was included in a corner of the image.

Image series were assembled into a three-dimensional array; hence, each image series was assembled with 90,000 intensity variations. A set of three descriptors (range, Fujii and wavelet entropy) obtained in the previous experiment was used to train and test a naïve Bayes model. Note that Fig. 3 shows the kernel density function estimated for each descriptor for one of the classes (bruised area).

We computed the values of the three chosen descriptors for each pixel of the training set of 100 images. For the DWT calculation we used the Daubechies order 2 with five levels of decomposition.

In Fig. 4 we show images of a bruised apple sample used as a training set employing different descriptors: (a) DWT Shannon entropy descriptor, (b) range descriptor, and (c) Fujii descriptor. The colored bar shows the image intensity scale. In this sample the bruised region is located at the middle bottom; meanwhile, the inert part is the right upper corner.

RGB images, colored according to the value of the density estimation function for each class (bruised, healthy and inert), are shown in Fig. 5, where the red plane stands for the bruised area, the green plane stands for the healthy tissue, and the blue plane stands for an inert region corresponding to a small metal piece introduced in the image field.

It can be seen that the inert, bruised, and healthy regions are clearly distinguished. These results

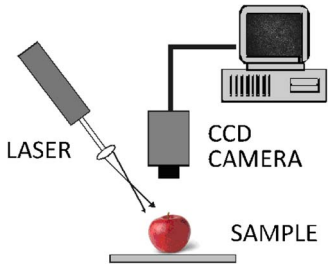

Fig. 2. (Color online) Experimental set up for the recording of biospeckle images.

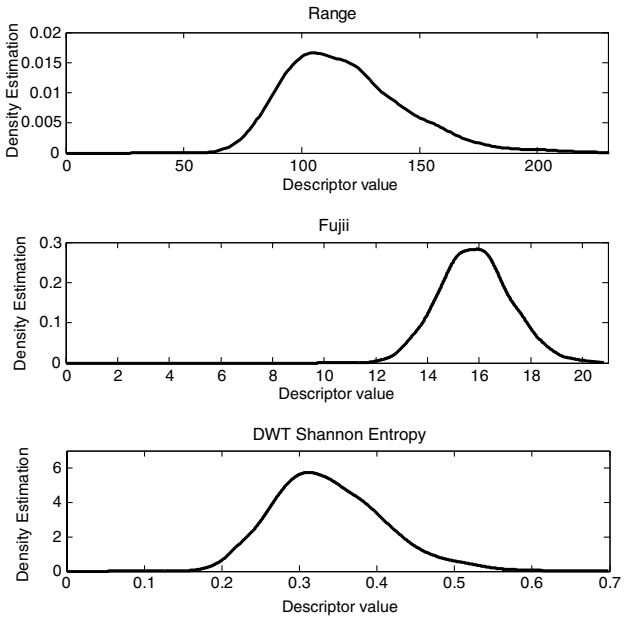

Fig. 3. Estimated probability density functions of the three chosen descriptors for the bruised region of the training sample.

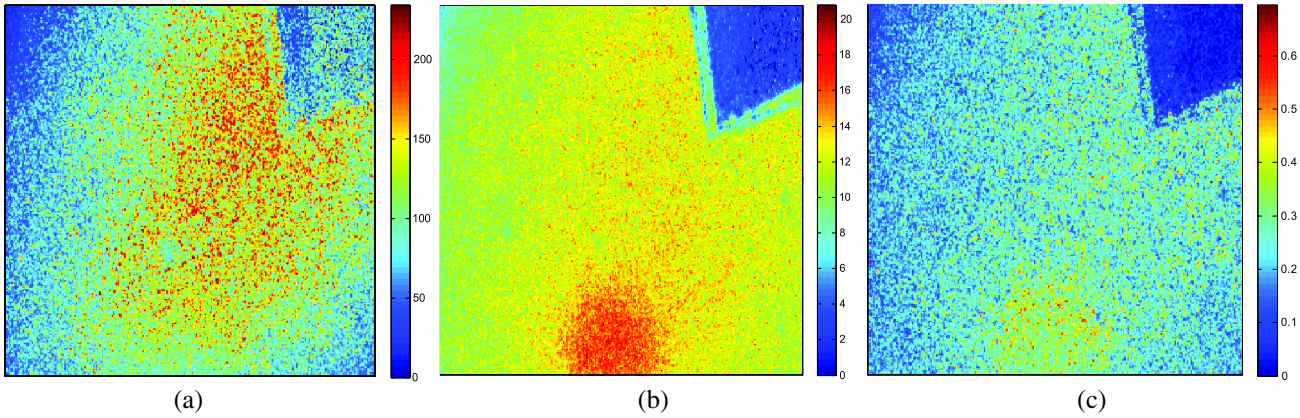

Fig. 4. Descriptor images of a bruised apple sample used as the training set: (a) DWT Shannon Entropy descriptor; (b) Range descriptor; (c) Fujii descriptor. The color bar shows the image intensity scale. In this sample the bruised region is located at the middle bottom and the inert part is in the right upper corner.

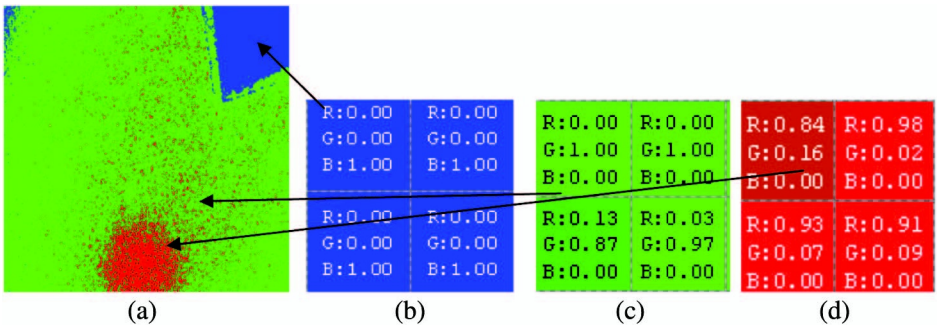

Fig. 5. (a) RGB image created with the results of computing the Bayesian model of the sample in Figure 4. Blue plane is associated with the inert region, the green plane with the healthy region and the red plane the bruised region. (b), (c) and (d) composition of four expanded pixels.

are consistent with those previously obtained from similar experiments in the past (see references).

After computing the *a posteriori* probability for each class $P(c_k/\mathbf{d})$ [Eq. (5)], we proposed the assignment of each pixel to that class (bruised, healthy, or inert area) that achieves the MAP. Combining the probabilistic model with the MAP decision rule (a thresholding operation), we obtained the results of the naïve Bayes classifier. The results are shown in Fig. 6. In these images the red regions indicate bruising, the blue area indicates the inert regions, and the green areas indicate the healthy regions. In addition to the already-known regions that here are well identified, there is a region with unknown activity origin, a line following the border of the knife edge used as an inert object in the right upper part, that has not been previously identified (Fig. 7 in [5]). It is now clearly identified as light coming from a reflection that belongs to one of the learned categories (the healthy class).

After this characterization as a learning step, the probabilities were calculated for an (assumed unknown) different set of images in a similar situation of bruising in a different apple, but in this case we removed the inert region.

The results are shown in Fig. 7. The (previously assumed unknown) bruising region of the sample is correctly identified. Notice that there are no blue regions because there was no inert region in the object. Its removal did not introduce any confusion in the results.

In order to validate our naïve Bayes classifier, a *tenfold cross-validation* method was used [21]. As a result, the initial data set, extracted from five different images of bruised apples, is divided into 10 subsets. These sets contain cases of the three classes: bruised, healthy, and inert apple regions. From these sets only one subset is retained as the validation data

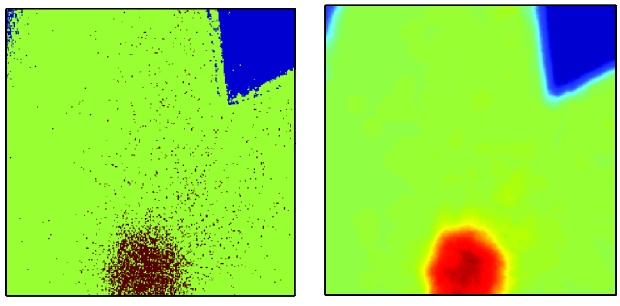

Fig. 6. Naïve Bayes classifier applied to the sample shown in Figure 5 (training set): (a) results of the Naïve Bayes classifier and (b) blurred version of figure (a).

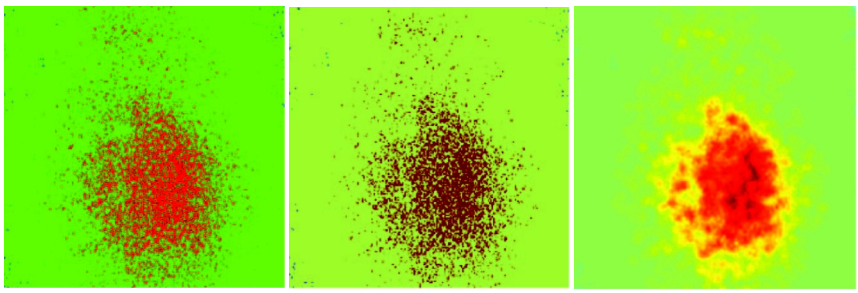

(a) (b) (c)

Fig. 7. Results of a testing case. The Naïve Bayes classifier discovers a bruised area in another apple sample not used in the training phase (assumed unknown). (a) RGB image, (b) Naïve Bayes classifier image, and (c) blurred image of the Naïve Bayes classifier.

Table 1. Confusion Matrix Showing How Many Pixels of Each Class are Correctly Identified (as a Percentage) in the Principal Diagonal[a]

		Predicted Areas			
		Bruised	Healthy	Inert	Sums
True areas	Bruised	7.13	1.98	0	9.12
	Healthy	2.25	80.81	0	83.07
	Inert	0	0.005	7.81	7.82
	Sums	9.39	82.80	7.81	100

[a]The other elements of the matrix show how the incorrectly detected pixels are distributed in the other classes.

for testing the model, and the other nine subsets are used for training purposes.

Each cross-validation process is repeated 10 times, with each of the 10 subsamples used once as a validation set. Then, we obtained 10 results from the validations, which we combined into a confusion matrix (Table 1). The confusion matrix is shown as the percentages of each pixel quantity over the whole sample.

A set of measurements on this confusion matrix is performed to assess the model's quality. Accuracy is the most commonly used metric to evaluate the performance of a classifier: it is the probability of new cases being correctly classified. If the confusion matrix is given as a number of events, the accuracy is computed as the sum of the principal diagonal elements divided by the total number of events. In our case the achieved accuracy is 95.75%. The Sensitivity or true positive rate represents the proportion of items classified as belonging to a certain class, from the total number of events that really belong to this class. This index is computed using the principal diagonal item of the confusion matrix divided by the sum of all elements of the row. The proposed model achieves a sensitivity for detecting a *bruised* area equal to 0.78, computed sensitivity to detect a *healthy* region is 0.97, and that for the *inert* zone is 0.99.

The precision for each class is defined in terms of the proportion of items that should actually belong to the class from among all the objects that are classified into this class. In the confusion matrix it is the respective principal diagonal value divided by the sum of the predicted class column. In our model the precisions for the different classes are bruised area = 0.7598, healthy area = 0.9760, and inert area = 1.

4. Conclusions

We have proposed the use of the naïve Bayes inference model to combine more than one biospeckle descriptor to segment areas of sample images in the evaluation of dynamic laser speckle image sequences. The independence of the naïve Bayes probabilistic model cannot be warranted for all descriptors and all types of samples and requires some heuristic testing. Once a probabilistic model is obtained, the evaluation of other samples, measured under similar conditions, can be successfully and rapidly achieved.

We have shown some results to illustrate the use of the probability images. The use of this technique has already found application in biology to distinguish bacteria from fungi, where successful results have also been obtained [22,23], as well as in agriculture for measuring the proportions of phases of endosperm in seeds (currently under development).

We expect that this procedure can be combined with the use of self-organized maps [24] to investigate samples in cases where no learning procedure is available. The authors have already experimented with unsupervised classifiers (self-organizing neural networks), where no supervised training samples are needed, which leads to the classification after stage labeling. These results will be reported elsewhere [25].

This work was supported by grant PICT 2008-1430 from the Agencia Nacional de Promoción en Ciencia y Tecnología (ANPCyT), Consejo Nacional de Investigaciones Científicas y Técnicas (CONICET), Comisión de Investigaciones Científicas de la Provincia de Buenos Aires (CIC), Universidad Nacional de Mar del Plata (UNMDP), and the Universidad Nacional de La Plata (UNLP), Argentina.

References

1. H. Rabal and R. Braga, eds., *Dynamic Laser Speckle and Applications* (CRS, Taylor & Francis, 2008).
2. R. M. Haralick, K. Shanmugan, and I. Dinstein, "Textural features for image classification," IEEE Trans. Syst. Man Cybern. **3**, 610–621 (1973).

3. G. H. Sendra, H. J. Rabal, R. Arizaga, and M. Trivi, "Biospeckle images decomposition in temporary spectral bands," Opt. Lett. **30**, 1641–1643 (2005).
4. H. Fujii, T. Asakura, K. Nohira, Y. Shintomi, and T. Ohura, "Blood flow observed by time varying speckle," Opt. Lett. **10**, 104–106 (1985).
5. I. Passoni, A. Dai Pra, H. Rabal, M. Trivi, and R. Arizaga, "Dynamic speckle processing using wavelets based entropy," Opt. Commun. **246**, 219–228 (2005).
6. A. Dai Pra, I. Passoni, and H. Rabal, "Evaluation of laser dynamic speckle signals applying granular computing," Signal Process. **89**, 266–274 (2009).
7. E. Blotta, V. Ballarin, and H. Rabal, "Decomposition of biospeckle signals through granulometric size distribution," Opt. Lett. **34**, 1201–1203 (2009).
8. I. Passoni, H. Rabal, and C. Arizmendi, "Characterizing dynamic speckle time series with the Hurst coefficient concept," Fractals **12**, 319–329 (2004).
9. G. H. Sendra, H. Rabal, R. Arizaga, and M. Trivi, "Vortex analysis in dynamic speckle images," J. Opt. Soc. Am. A **26**, 2634–2639 (2009).
10. H. Rabal, R. Arizaga, N. Cap, M. Trivi, G. Romero, and E. Alanís, "Transient phenomena analysis using dynamic speckle patterns," Opt. Eng. **35**, 57–62 (1996).
11. G. Romero, E. Alanis, and H. Rabal, "Statistics of the dynamic speckle produced by a rotating diffuser and its application to the assessment of paint drying," Opt. Eng. **39**, 1652–1658 (2000).
12. M. Pajuelo, G. Baldwin, R. Arizaga, N. Cap, H. Rabal, and M. Trivi, "Bio-speckle assessment of bruising in fruits," Opt. Lasers Eng. **40**, 13–24 (2003).
13. A. Federico and G. Kaufmann, "Evaluation of dynamic speckle activity using the empirical mode decomposition method," Opt. Commun. **267**, 287–294 (2006).
14. J. D. Briers and S. Webster, "Laser speckle contrast analysis (LASCA): a nonscanning full field technique for monitoring capillary blood flow," J. Biomed. Opt. **1**, 174–179 (1996).
15. G. H. Sendra, A. L. Dai Pra, L. I. Passoni, R. Arizaga, H. J. Rabal, and M. Triv, "Biospeckle descriptors: a performance comparison," Proc. SPIE **7387**, 73871K (2010).
16. H. Z. Cummins and H. L. Swinney, "Light beating spectroscopy," in Vol. **8** of *Progress in Optics* (North-Holland, 1970), pp. 133–200.
17. E. Blotta, V. Ballarín, M. Brun, and H. Rabal, "Evaluation of speckle-interferometry descriptors to measuring drying-of-coatings," Signal Process. **91**, 2395–2403 (2011).
18. I. Rish, "An empirical study of the naive Bayes classifier," in RC 22230 IBM Research Report. IBM Research Division (Thomas J. Watson Research Center, Yorktown Heights, NY, 2001).
19. E. Parzen, "On estimation of a probability function and mode," Ann. Math. Stat. **33**, 1065–1076 (1962).
20. R. Kohavi and G. H. John, "Wrappers for feature subset selection," Artif. Intell. **97**, 273–324 (1997).
21. M. Stone, "Cross-validatory choice and assessment of statistical predictions," J. R. Stat. Soc. **36**, 111–147 (1974).
22. S. Murialdo, L. Passoni, M. Guzman, G. Sendra, H. Rabal, M. Trivi, and J. Froilán Gonzalez, "Discrimination of motile bacteria and filamentous fungi using dynamic speckle," J. Biomed. Opt. **17**, 056011 (2012).
23. G. Meschino, S. Murialdo, L. Passoni, H. Rabal, and M. Trivi, "Biospeckle image stack process based on artificial neural networks," in *Proceedings of the 32nd Annual International Conference of the IEEE Engineering in Medicine and Biology Society* (IEEE, 2010), pp. 4056–4059.
24. M. Guzmán, G. Meschino, A. L. Dai Pra, L. Passoni, H. Rabal, and M. Trivi, "Dynamic laser speckle: decision models with computational intelligence techniques," Proc. SPIE **7387**, 738717 (2010).
25. L. I. Passoni, A. L. Dai Pra, A. Scandurra, G. Meschino, C. Weber, M. Guzmán, H. Rabal, and M. Trivi, "Improvements in the visualization of segmented areas of patterns of dynamic laser speckle in advances in self-organizing maps," in *Advances in Intelligent Systems and Computing*, P. A. Estévez, J. C. Príncipe, and P. Zegers, eds. (Springer, 2012), pp. 163–171.